J Mater Sci (2008) 43:1783–1794
DOI 10.1007/s10853-007-2398-8

Fatigue crack orientation in NR and SBR under variable amplitude and multiaxial loading conditions

Ryan J. Harbour · Ali Fatemi · Will V. Mars

Received: 31 January 2007 / Accepted: 10 December 2007 / Published online: 18 January 2008

Abstract The orientations of cracks as they develop in a material indicate the planes that have experienced the maximum damage. For the purpose of fatigue life analysis and prediction, these planes are referred to as the failure or critical planes. In order to study the planes on which cracks develop for different types of loading, the development of cracks was observed during constant and variable amplitude experiments using the multiaxial ring specimen. Two filled rubber materials were compared in this study: NR, which strain crystallizes, and SBR, which does not. Multiaxial test signals composed of alternating blocks of axial and torsion cycles (each of which acts on different critical planes) produced crack orientations that fell between those occurring for signals composed only of axial or of torsion cycles. Plane-specific fatigue damage parameters of cracking energy density and normal strain were evaluated for their ability to predict the experimentally observed planes of crack development.

R. J. Harbour
The University of Toledo, Toledo, OH, USA

Present Address:
R. J. Harbour
Goodyear Tire and Rubber Company, Akron, OH, USA

A. Fatemi (✉)
Mechanical, Industrial and Manufacturing Engineering Department, The University of Toledo, 2801 West Bancroft Street, Toledo, OH 43606, USA
e-mail: afatemi@eng.utoledo.edu

W. V. Mars
Research Department, Cooper Tire and Rubber Company, 701 Lima Avenue, Findlay, OH 45840, USA
e-mail: wvmars@coopertire.com

Nomenclature

$\vec{r}$	Unit normal vector
T_{Wc}	Energy release rate based on cracking energy density
W	Strain energy density
W_{NH}	Strain energy density based on Neo–Hookean model
W_c	Cracking energy density
$W_{c,raw}$	Raw computed cracking energy density
α	Angle of crack orientation from horizontal plane
$\boldsymbol{\varepsilon}$, ε	Strain tensor, state of strain
ε_n	Normal strain
σ	State of stress
ϕ	Angle of crack plane in material thickness direction

Introduction

The ability of rubber to withstand large strains without being permanently deformed has made it a popular material choice for many manufactured products. Due to this wide range of product usage, rubber experiences a wide variety of loading conditions. Realistic service load histories for these rubber components almost always involve variable amplitude loading conditions. In order to improve the durability of rubber components and the methods used to analyze and predict fatigue behavior for the material, a better understanding of the effects of variable amplitude loading conditions on the development and growth of fatigue cracks is necessary.

Although research has been conducted to study the fatigue behavior of rubber, they have generally focused on constant amplitude loading conditions. Limited research [1–4] has been published dealing with the effect of specific

aspects of variable amplitude loading conditions on constitutive behavior and fatigue lives, but the effects of variable amplitude loading conditions on crack development and growth has not been thoroughly discussed in these studies.

Mars and Fatemi studied crack orientation [5] and crack growth [6] during their constant amplitude experiments with natural rubber. They observed that the orientation of cracks was not random in the specimen, but was a result of the type of loading being applied. For example, pure axial tests produced only horizontal cracks and torsion tests tended to produce angled cracks. They used the plane-specific parameter of cracking energy density to successfully predict the material planes that experienced the most damage. Crack growth rates were measured from the crack growth histories obtained during these tests. The crack growth rate results were tabulated against multiple forms of energy release rate and found to fall below the crack growth rate results measured from a pure shear specimen. The work presented in this article was designed to extend the work of Mars and Fatemi related to crack orientation and crack growth under constant amplitude loading to variable amplitude loading.

The goal of the fatigue experiments described in this work was to investigate the effects of variable amplitude loading conditions on the fatigue behavior of filled rubbers. Since actual service load histories are generally variable in nature, the effects associated with variable amplitude loading conditions can have significant implications in most applications. While many aspects of fatigue behavior were considered during this study, this article focuses on the development and growth of cracks in the specimen. The variable amplitude test signals were selected to simulate some common aspects from actual load histories. The results from the variable amplitude experiments were used to determine the applicability of plane-specific damage parameters for predicting crack orientations and a linear crack growth rate prediction model that utilizes crack growth rate results from constant amplitude crack growth tests to predict variable amplitude fatigue crack growth rates.

This article begins with an overview of the experimental program including the materials and specimen used as well as experimental procedures. Next, the observed crack development in the specimens is presented and the results from the different materials are compared. Then, the plane-specific parameters of cracking energy density and normal strain are used to predict crack orientations and these predictions are compared to the observed results. This is followed by a comparison of the measured crack growth rates for the multiaxial ring specimen and the crack growth rate results from pure shear specimens. A linear crack growth rate model is then used to predict the variable amplitude fatigue crack growth rates for the multiaxial ring specimen based on the constant amplitude crack growth rate results.

Experimental program

Materials

The experiments used specimens molded from both filled natural rubber (NR) and filled styrene–butadiene rubber (SBR) compounds (recipes provided in Table 1). The filler loadings were selected to produce roughly the same compound stiffness levels. NR strain crystallizes, which refers to a phase transformation that some elastomers experience due to the application of strain, while SBR does not. Strain crystallization [7] can significantly affect both the strength of the material and its fatigue properties.

Test specimen

The experiments used the multiaxial ring specimen designed by Mars and Fatemi [8] for a wide range of multiaxial loading conditions. The specimen consists of a rubber ring bonded between two steel mounting rings, as illustrated in Fig. 1. This test specimen experiences normal and shear strains during the application of simultaneous axial and twist displacements to the specimen. The cross-section of the specimen is designed to produce maximum stress on the outer surface of the specimen in order to allow for the monitoring of crack development during the experiments. Silver ink applied to the specimen helped to enhance the visibility of the developing cracks.

Test load signals

The test signals used with the multiaxial ring specimen consisted of both constant and variable amplitude signals. The test paths are represented graphically in terms of applied axial displacement and rotational twist, in Fig. 2, with the axial displacements on the horizontal axis and the rotational twist on the vertical axis. For the constant amplitude tests (paths A–E) that consist of a single loading condition, a single bar represents the path of deformation. For the variable amplitude tests (paths F–I) that consist of alternating blocks of constant amplitude cycles that combine to form a test sequence, each bar denotes the path of deformation for an individual block of cycles. The experimental plan also included a more complex variable amplitude test signal that involved combined axial and torsional displacements applied in a random order (path J). It is important to note that the letter designations for test

Table 1 Recipes for filled NR and filled SBR compounds

Ingredient	Filled NR		Filled SBR	
	PHR[a]	% of weight	PHR[a]	% of weight
NR	100	53.7		
SBR rubber cold, dry, NST (SBR 1502)			100	50.5
Carbon black, N234			75	37.9
Carbon black, N650	60	32.2		
Aromatic petroleum hydrocarbon oil	2	1.1	15	7.6
Zinc oxide	8	4.3	3	1.5
Resorcinol donor	3	1.6		
Stearic acid, rubber grade	2	1.1	1	0.5
Sulfur, elemental			1.8	0.9
Tert butyl benzothiazole sulfenamide (TBBS)			1.4	0.7
Polymerized 1,2-dihydro-2,2,4-trimethylquinoline (TMQ)	1	0.5	1	0.5
CO Neodeconaoate	0.5	0.3		
Sulfur 20% naphthenic base oil	4.5	2.4		
Melamine formaldehyde resin on a silica carrier	4.2	2.2		
DCBS	0.8	0.4		
N-(Cyclohexylthio) phthalimide (PVI)	0.2	0.1		
Total parts per hundred rubber	186.0	100.0	198.2	100.0

[a] Parts per hundred rubber, by weight

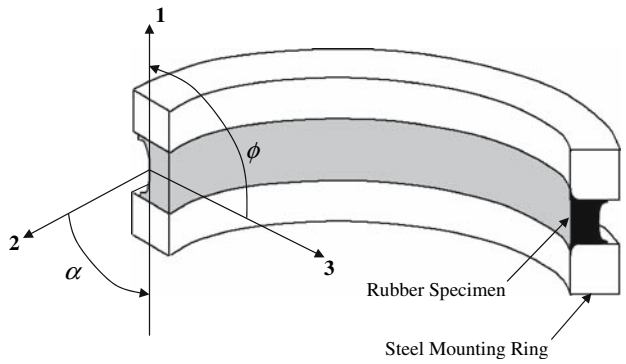

Fig. 1 Multiaxial ring test specimen with crack orientation definitions: α represents the angle of the cracking plane within the surface plane (1 and 2 directions) and ϕ represents the angle of crack growth into the material (1 and 3 directions)

paths in this study do not correspond to the test path designations of Mars and Fatemi [4].

During the application of all torsional cycles during this investigation, the axial displacement was constrained to zero producing a non-zero axial load in the specimen. This method of applying torsional cycles was utilized to be consistent with the experiments conducted by Mars and Fatemi [4].

The constant amplitude tests focused on pure axial and torsion constant amplitude tests since Mars and Fatemi [4] found these loading conditions to be the boundary cases in terms of axial–torsion fatigue life. The results from proportional and non-proportional axial–torsion test signals generally fell between the pure axial and torsion tests on fatigue life plots. In this study, path A designates a pure axial test with $R_\delta = 0$ and a twist angle of zero. Paths B and C represent torsion tests for different values of R_θ and axial displacements maintained at zero. R_δ and R_θ represent the ratio of the minimum to the maximum displacement for axial and torsion cycles, respectively. Path B was for torsion with a minimum twist angle of zero ($R_\theta = 0$) and path C was for fully reversed torsion ($R_\theta = -1$). A limited number of fully reversed torsion tests were also conducted with static axial displacements to investigate the effects of static axial displacements on the fatigue behavior during torsion tests. Path D applied a tensile static displacement and path E applied a static compressive displacement.

The variable amplitude load signals consisted of multilevel and multiaxial tests. The multilevel test signals (paths F and G) consisted of two blocks with different peak strain levels for the same type of loading: axial or torsion. These signals investigated the effects of variable amplitude loading on material behavior when the planes of crack growth for each component of the signal were the same. Path F involved multiple levels of axial displacement with a constant twist angle of zero. Similarly, path G involved multiple levels of fully reversed torsion while holding the axial displacement at the zero level.

The multiaxial signals (paths H and I) consisted of alternating blocks of axial and torsion cycles designed to study the effects of variable amplitude loading in multiaxial experiments. The fact that pure axial and torsion tests generally produced cracks on different planes was the reason for using these loading conditions in the multiaxial

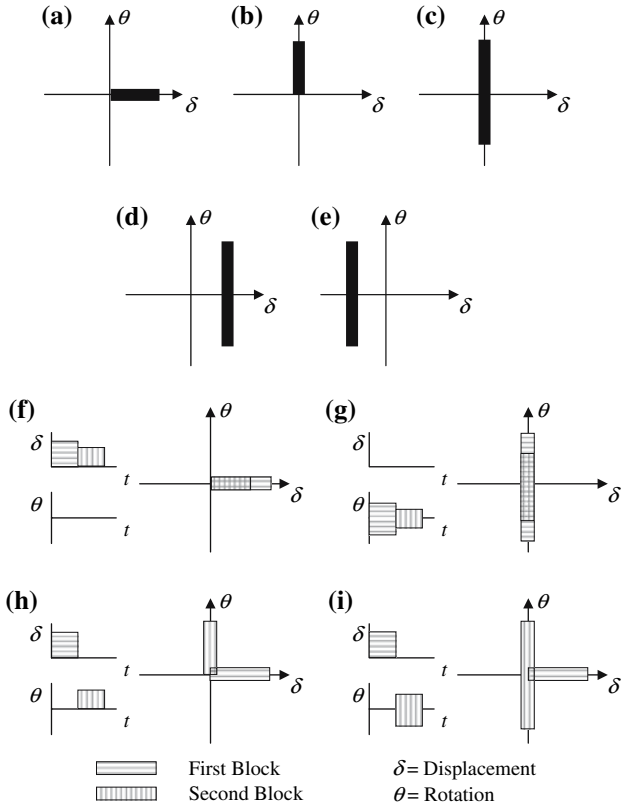

Fig. 2 Displacement test paths for constant amplitude tests (paths A through E) and variable amplitude tests (paths F through I) with axial displacement on the horizontal axis and rotational twist on the vertical axis. For variable amplitude signals, each bar represents the path of deformation for an individual block of cycles from the test sequence

test signals. Path H consisted of axial cycles alternating with torsion cycles at $R_\theta = 0$ while path I alternated axial cycles with fully reversed torsion cycles. For some multiaxial paths, the relative number of applied cycles during the axial and torsion blocks differed between tests in order to vary the dominant axis of loading.

Crack orientation observations

The orientation of a crack in the multiaxial ring specimen is defined using the angles α and ϕ as illustrated in Fig. 1. The α angle represents the crack direction within the surface plane of the specimen measured from the horizontal plane in a counter-clockwise direction. The ϕ angle represents the direction of crack growth into the material from the horizontal plane. These two angles completely specify crack orientation. Due to symmetry, all orientations can be represented by α ranging from 0° to 180° and ϕ ranging from −90° to 90°. Physical inspection of sections cut from cracked specimens for multiple test paths in both materials showed that cracks tended to grow along the direction of $\phi = 0$. While the critical crack planes for the tests in this investigation were for $\phi = 0$, this would not be the case for tests that contain significant compressive cycles since cracks for these tests would tend to form along shear planes that do not correspond to $\phi = 0$.

Observed crack orientations

A digital camera mounted to a pivoting arm on the test machine took pictures of the specimen at various points during each test. The analysis of the digital images captured during each experiment provided data regarding the development and growth of cracks on the surface of the specimen. Since tests produced multiple cracks on the surface of the specimen, a range of angles is used to identify the orientations at which the different cracks developed. Angled cracks generally had variations in orientation of 10–15°. Inspection of the specimens allowed the densities of cracks to be estimated for each test and categorized based on the number of visible cracks present on the entire surface of the specimen at the time of failure. NR tended to develop a high crack density, while SBR tended to have lower crack densities. The difference in crack density between the two materials was attributed to size and density of initial flaws in the materials based on inspection of the materials using a scanning electron microscope. This is further discussed in the "Comparison of crack development in NR and SBR" section.

The common types of observed cracks included horizontal cracks, angled cracks, multi-angled cracks, and combined cracks. Angled cracks refer to the cases where the cracks develop for only the positive range of angles while multi-angled cracks refer to the cases that produce cracks for both the positive and negative range of angles (such as star cracks). Combined cracks developed as both horizontal and angled cracks. For combined cracks, generally one type of crack had the higher density of cracks and grew longer. This type of crack was referred to as the dominant crack type for the combined cracks. When individual cracks grew together and formed a single larger crack, the cracks had coalesced. This new crack was regarded as a single crack in terms of crack length measurements.

Constant amplitude tests

The crack length histories for all of the test paths in both materials showed similar trends. Once a crack was visible in the specimen, the crack initially grew slowly. As the crack in the specimen increased in length, the rate of crack growth increased. This faster rate of crack growth is expected since the driving force for crack growth is a function of crack length.

Typical crack images are shown in Fig. 3 for paths A–C in both materials. Pure axial tests (path A) produced horizontal cracks. The NR specimens generally developed a large number of cracks that eventually coalesced to form larger cracks. The SBR specimens tended to only produce a couple of horizontal cracks that grew significantly longer (beyond 10 mm) than the cracks in NR and had less of a tendency to coalesce since there were fewer cracks. The torsion tests with $R_\theta = 0$ (path B) produced mostly angled cracks in the range of 40–50° for both materials. While the angled cracks represented the majority of the cracks in SBR, a limited number of horizontal cracks also developed in the specimens.

For fully reversed torsion tests (path C), the results differed for the two materials. The cracks in NR generally developed as combined cracks. Horizontal cracks dominated the surfaces of the specimens, but angled cracks in the ranges of 40–50° and −40° to −50° also were observed in the specimen. The angled cracks tended to develop at the ends of horizontal cracks in the specimen. Friction between the inner surfaces of the horizontal cracks during the twisting motion wore at the material and caused loose rubber particles to collect on the surface of the specimen at the crack tips. The fully reversed torsion tests in SBR also developed cracks in the range of 40–50° and −40° to −50°, but did not produce any horizontal cracks. The angled cracks commonly crossed each other to produce x-shaped cracks sometimes referred to as star cracks.

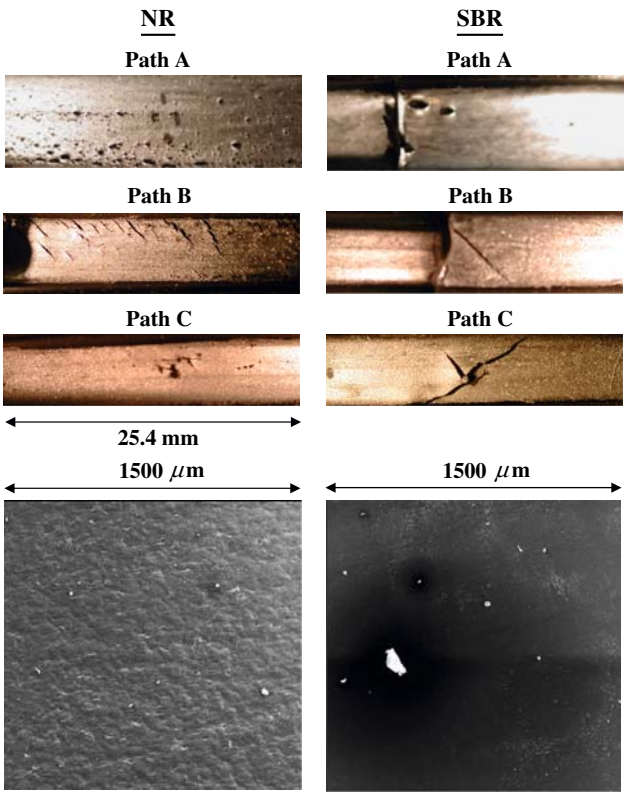

Fig. 3 Typical crack orientations for load paths A–C along with microscopic images of initial flaws in untested specimens for (*left*) NR and (*right*) SBR

Mars and Fatemi [5] observed similar crack development during their experiments with NR using multiaxial ring specimens. The observed crack densities for their tests were similar to those described from this study with a high number of cracks developing over the entire specimen. For paths A and B, they observed horizontal cracks and angled cracks very similar to those pictured in Fig. 3 for NR. However, the observed cracks differed for fully reversed torsion tests (path C). They observed angled cracks in both the positive and negative directions, but the specimens from this study exhibited mostly horizontal cracks with only a few angled cracks developing off of the horizontal cracks. A likely source for this observed difference in crack development between the two studies would be differences in the initial flaw size and density in the material that could be attributed to the specimens being manufactured at different facilities. It is suspected that slightly different material preparation and specimen-manufacturing techniques between the two facilities could have produced specimens with different initial flaw size and density. Two possible sources of these material variations are different degrees of mixing during compound preparation or different levels of air becoming entrapped in the material to produce voids in the material during the preparation process. Since the growth of these flaws produce the observed cracks, differences in the initial flaw size of the different material batches could cause specimens to produce different types of cracks for the same loading conditions.

The remaining constant amplitude tests (paths D and E) produced similar types of cracks in both materials. The fully reversed torsion tests with static tensile displacements developed multi-angled cracks in both materials. The fully reversed torsion tests with static compressive displacements exhibited horizontal cracks that sheared the specimen in half along the center of the specimen. It appeared that the compressive levels in the specimen caused wrinkling. It also appeared that the friction related to the twisting motion combined with the compressive displacements caused increased temperatures in the specimen.

The multilevel tests (paths F and G) developed similar crack orientations as the corresponding constant amplitude tests in both materials. The multilevel axial tests (path F) produced horizontal cracks in both materials while the multilevel torsion tests (path G) produced dominant horizontal cracks in NR and mostly angled cracks in SBR between 30° and 50° in both the positive and negative directions.

Multiaxial tests

Test signals that combined alternating blocks of axial and torsion with $R_\theta = 0$ cycles (path H) in NR produced angled cracks between 5° and 30°. The observed range of crack orientations was found to be dependent on the relative number of axial and torsional cycles in the test sequence for the same strain levels of each type of cycle. This dependence on the relative number of cycles is illustrated in Fig. 4. Experiments with higher numbers of axial cycles produced cracks with generally smaller angles (5–20°). The angles of crack orientation became steeper (15–30°) as the test sequences included higher numbers of torsional cycles. Tests for path H in SBR exhibited similar effects on crack orientation based on the relative number of axial and torsional cycles. One difference from NR for test path H was the type of cracks that formed in SBR. While NR formed angled cracks for just the positive angles as was expected, SBR also developed cracks for the negative angles resulting in x-shaped cracks on the surface of the specimen. This could be caused by the interaction of the different developing cracks in the SBR specimen causing additional cracks to form in the other directions. Since SBR tended to develop only a few cracks that grew much longer than those in NR, additional cracks tended to grow between the larger initial cracks in SBR. The applied axial cycles would help to propagate any cracks that developed off of the original cracks. For NR, the high number of small cracks tended to promote the coalescing of cracks due to the shorter crack lengths.

The multiaxial tests for path I in NR consisted of alternating blocks of axial and fully reversed torsion cycles that both dominantly produced horizontal cracks during the constant amplitude tests. As was expected, the corresponding multiaxial tests also produced horizontal cracks in NR. For test path I in SBR, a combination of horizontal and multi-angled cracks developed on the surface of the specimen with the angled cracks being the dominant cracks. The number of axial and fully reversed torsion cycles per sequence had similar effects on the orientations of the multi-angled cracks to those observed for test path H in both materials. This dependence observed for test path I in SBR is illustrated in Fig. 5. For test path I in SBR, increasing the ratio of axial cycles reduced the angle of the cracks. Similarly, adding more torsional cycles resulted in larger angles of crack orientation.

On the basis of the results for the multiaxial test signals, the angle of crack orientation for a signal that combines cycles that act on different planes under constant amplitude conditions can generally be represented as a weighted average of the angles of crack orientation for each cyclic component assuming similar strain levels for each component. The maximum accumulated damage for the test sequence occurs on a different plane than the maximum damage levels for each individual cycle. The summation of lesser damage levels on another plane produces a greater

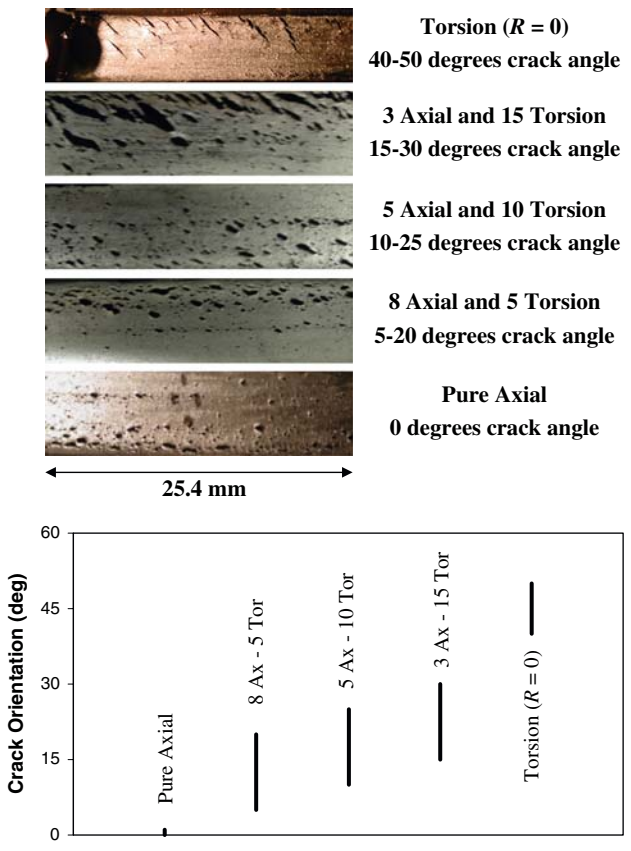

Fig. 4 Comparison of typical crack orientation near the end of specimen life for different numbers of axial and torsional cycles while maintaining the same relative strain levels in test path H for NR along with sample crack images. Pure axial (path A) and torsional (path B) tests are included for reference

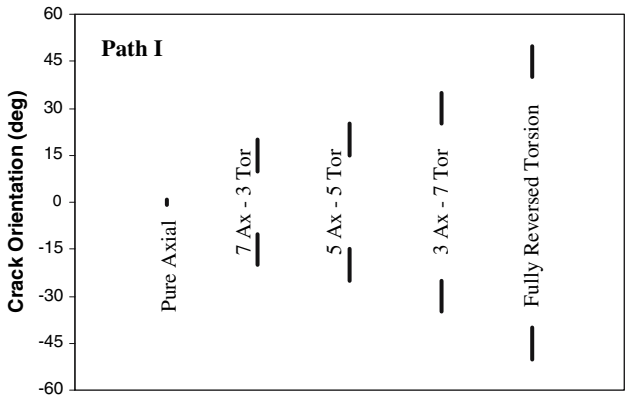

Fig. 5 Comparison of typical crack orientation near the end of specimen life for different numbers of axial and torsional cycles for multiaxial test path I in SBR. Pure axial (path A) and torsional (path C) tests are included for reference

accumulated damage than the damage done on either of the individual maximum damage planes.

Comparison of crack development in NR and SBR

The higher densities of cracks that develop in NR as compared to SBR, as shown in Fig. 3, have been attributed to differences in the size and density of initial flaws in the material as previously noted. The microscopic images captured of untested specimens in Fig. 3 show that the NR specimen tends to have a high density of smaller initial flaws while SBR has a few larger inclusions as indicated by the white spots in the images. In NR, the high density of similarly sized flaws would result in numerous cracks nucleating at the same time. These cracks would still be relatively small at the point of failure for a stiffness-based failure criterion since the combined effect of the many small cracks would be enough to produce the necessary drop in stiffness. The fewer large inclusions in SBR would produce fewer cracks that need to grow longer in order to cause the same drop in stiffness.

While the orientation of cracks on the surface of the specimens was generally found to be consistent in both materials for each test signal, the orientations did vary between materials for some tests. The main difference between the materials with regards to crack orientation was for the tests that included fully reversed torsion cycles. These tests produced mostly multi-angled cracks in SBR while the majority of the cracks for these tests in NR were horizontal cracks. For multiaxial tests that combined axial and torsional cycles that acted on different cracking planes, both materials exhibited similar sensitivities to the number of axial and torsional cycles per sequence.

Crack orientation predictions

Crack orientations were predicted using two plane-specific, i.e. critical plane, equivalence parameters: cracking energy density and normal strain. This section presents the details of these predictions for various tests followed by a comparison of the predicted and experimental crack orientations for each parameter. Predicting critical planes for variable amplitude loading conditions requires the use of a cycle counting procedure and damage accumulation model to determine the planes that experience the maximum accumulated damage. The plane of maximum accumulated damage defines the predicted crack orientation for each experiment since it directly corresponds to the plane of minimum fatigue life. Once the critical plane is identified, the accumulated damage on that plane can then be used for fatigue life prediction. While a single plane orientation experiences the maximum predicted damage, it is likely for cracks to develop and grow in any plane that experiences damage levels near the maximum value. On the basis of this idea, the range of crack orientations that experience 95% of the maximum predicted damage was also considered as possible critical plane orientations for each parameter. The critical plane always corresponds to $\phi = 0$ for all of the tests in this investigation. The calculations were carried out at 1° intervals for the α direction between the angles of 0° and 180° due to symmetry. For variable amplitude tests, Miner's [9] linear damage rule was applied on each plane to find the total accumulated damage per sequence.

Cracking energy density

Cracking energy density W_c represents the portion of the strain energy density that is available on a particular plane to be released through crack growth. Cracking energy density differs from the strain energy density in that the cracking energy density depends on the cracking plane orientation. Strain energy density is independent of plane orientation. Further details on cracking energy density are provided in [10].

The basic form of the cracking energy density increment dW_c is given by:

$$dW_c = \overrightarrow{r}^T \sigma d\varepsilon \overrightarrow{r} \quad (1)$$

where $\overrightarrow{r}$ is the crack orientation vector. The integration of this expression gives the cracking energy density for the given plane. In order to account for crack closure, compressive normal strains on a plane do not produce any cracking energy density since cracks are closed on the plane. Mars and Fatemi [10] describe the approach to calculating cracking energy density used in this study. Since cracking energy density is a positive definite parameter, the maximum and range for the parameter are equal for tests that pass through a fully unloaded state. On the basis of this observation, only the maximum value is used to predict crack orientation based on cracking energy density. For a fully reversed torsion cycle, Miner's linear damage rule is applied to accumulate the damage caused on each plane by both the positive and negative twist directions.

The damage levels as a function of plane orientation α based on cracking energy density are plotted in Fig. 6 through Fig. 8 for various test paths in SBR. The predicted crack orientation is defined as the plane of maximum damage from these plots. The predicted crack orientations for NR were similar to those presented for SBR. Figure 6 shows damage per cycle as a function of plane orientation for pure axial tests (path A) and torsion tests with $R_\theta = 0$

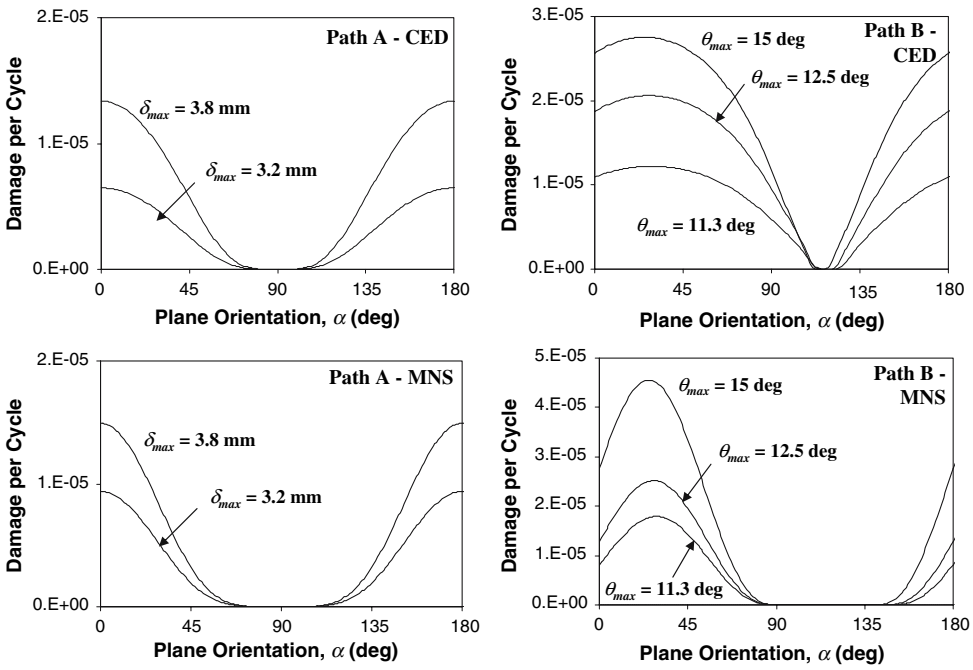

Fig. 6 Damage per cycle as a function of plane orientation for pure axial tests (path A) and torsion tests with $R_\theta = 0$ (path B) in SBR according to (*top*) cracking energy density and (*bottom*) maximum normal strain

(path B) for SBR. For path A, the maximum damage occurs on the zero-degree plane for each level of maximum displacement. The damage plots for torsion tests with $R_\theta = 0$ (path B) in Fig. 6 show the maximum damage in these tests vary from 30° to 25° for the maximum twist angles shown in the figure. The plane of maximum damage is dependent on the maximum twist angle since the normal strain becomes a larger influence at higher twist angles. As the twist angle increases, the plane of maximum damage shifts toward zero. Similarly, the plane of maximum damage shifts toward higher angles as the maximum twist angle decreases. The maximum accumulated damage per cycle for fully reversed torsion tests, shown in Fig. 7, occurs on the zero-degree plane, but the difference in damage between the maximum and minimum damage levels is smaller than for torsion tests with $R_\theta = 0$. The smaller difference between the minimum and the maximum levels of damage in the fully reversed torsion tests is a result of the superposition of the damage that occurs during the positive and the negative twist directions.

Mars and Fatemi [4] used a similar analysis based on cracking energy density to predict the planes of maximum damage for their NR experiments using the multiaxial ring specimen. While their predicted results were similar to this study for paths A and B, they assumed the plane that experiences the maximum damage for each direction of twist angle in path C would be a critical plane rather than using Miner's linear damage rule to find the plane or planes that experiences the largest accumulated damage over the entire cycle. While these two predicted crack orientations for path C differ significantly, actual results tend to reflect both predictions. Specimens subjected to path C tended to develop dominant horizontal cracks as well as angled cracks. Since Mars and Fatemi noted that their fully reversed torsion tests tended to develop mostly angled cracks, they concluded that cracking energy density did an acceptable job of predicting crack orientations for their tests.

As would be expected, since the multilevel tests (paths F and G) combine cycles that predict similar cracking planes under constant amplitude tests, cracking energy density predicts the same crack orientations for the multilevel tests as for the corresponding constant amplitude tests.

The accumulated damage results for test path H in Fig. 8 indicate that the plane of maximum accumulated damage falls between the zero-degree cracking plane for the pure axial cycles (path A) and the 25° cracking plane associated with the torsional cycles at $R_\theta = 0$ (path B). The only difference between the three signals for each material in Fig. 8 is the number of axial and torsional cycles per sequence. As the relative number of axial and torsional cycles increases in each sequence, the angle of the cracking plane becomes smaller, approaching zero degrees. The damage plots in Fig. 8 for path I that combines axial (path A) and fully reversed torsion (path C) cycles indicate maximum accumulated damage levels on the zero-degree plane as would be expected based on the constant amplitude test results.

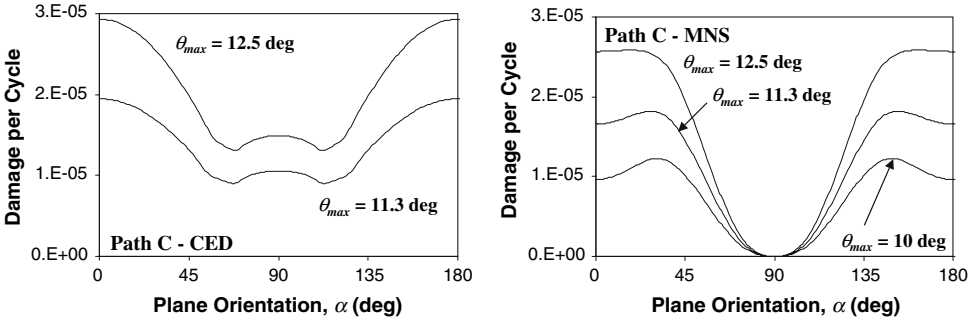

Fig. 7 Damage per cycle as a function of plane orientation for fully reversed torsion tests (path C) in SBR according to (*left*) cracking energy density and (*right*) maximum normal strain

Normal strain

The maximum principal strain can be applied as a scalar equivalence parameter [10]. Although this parameter has an associated direction which can be correlated to the plane of crack nucleation for some simple loading histories, it is not strictly a plane-specific approach since its direction is associated only with the instantaneous loading condition rather than the material in which developing cracks are embedded. In order to investigate the applicability of a strain-based parameter in a plane-specific approach, the normal strain acting on each plane was used as an equivalence parameter for multiaxial tests. The normal strain ε_n acting on a plane is given by the dot product:

$$\varepsilon_n = (\boldsymbol{\varepsilon}\vec{r}) \cdot \vec{r} \tag{2}$$

where $\boldsymbol{\varepsilon}$ is the strain tensor and $\vec{r}$ is the direction vector normal to the plane. For the plane normal to the maximum principal strain direction, the normal strain is equivalent to the maximum principal strain.

The normal strain approach predicts fatigue crack orientations using a similar planar analysis approach as the one described for cracking energy density. One difference between the approaches is that cracking energy density is a positive definite parameter while normal strain can produce negative values. For tests that pass through a fully relaxed point, the maximum value and range of values on a plane are the same for cracking energy density. This is not the case for normal strain since it can produce negative strains on a plane.

For the case of normal strain, valid arguments could be made for the use of either maximum or range. Since damage is not associated with compressive normal strains due to crack closure, the use of maximum normal strain would be appropriate for test paths that include compressive strains. However, maximum normal strain cannot distinguish between static and cyclic loadings when selecting the critical plane. Both approaches were considered in this investigation. The selection of which to use depends on the types of loading being analyzed. While this section focuses on the damage analysis for only the

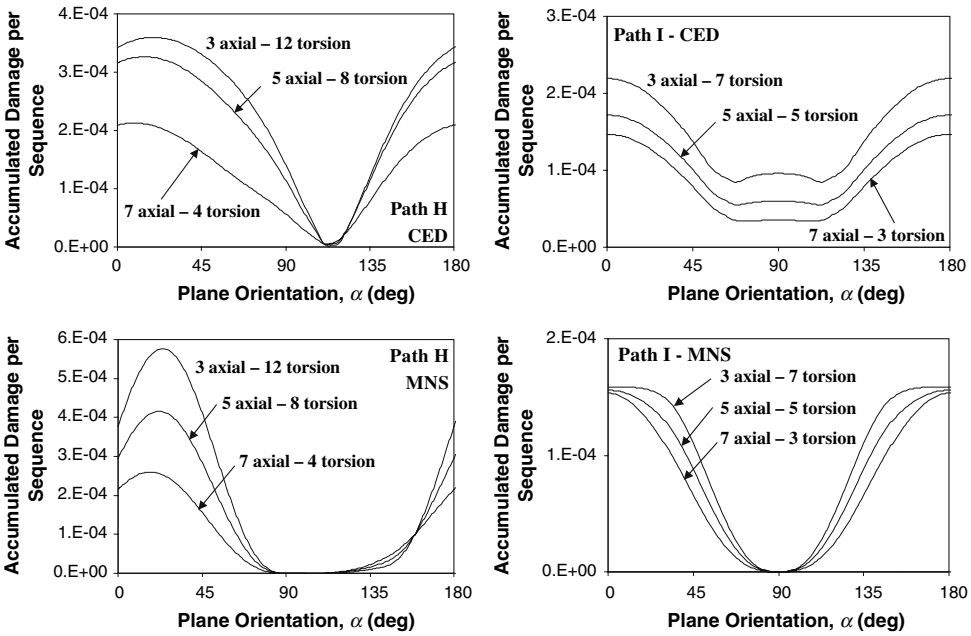

Fig. 8 Accumulated damage per sequence as a function of plane orientation for multiaxial test paths (*left*) H and (*right*) I in SBR according to (*top*) cracking energy density and (*bottom*) normal strain. The same axial and torsional displacements were used for the three signals for each path. The only difference between the signals is the number of axial and torsional cycles per sequence

maximum normal strain approach, the predicted crack orientations for both maximum normal strain and normal strain range are compared in the following section.

Figure 6 includes the damage plots for paths A and B in SBR only since the results are similar for NR for these paths. For path A, the maximum damage occurs on the zero-degree plane for all of the axial tests. For the torsion tests with $R_\theta = 0$ (path B), the maximum damage occurs between the angles of 25° and 30°, depending on the maximum twist angle as shown in Fig. 6. Similar to the cracking energy density results, the plane of maximum damage also decreases slightly as the twist angle increases. For larger twist angles, the plane of maximum damage would be expected to continue to decrease. For the fully reversed torsion cycles (path C) shown in Fig. 7, the plane of maximum damage shifts toward zero as the twist amplitude increases. The minimum applied twist angle of 10° predicts maximum damage for a crack orientation of 30°. The maximum twist angle of 12.5° predicts a crack orientation of 17°. The predicted crack orientation becomes zero as the twist amplitude approaches 13°. A similar pattern also occurs for the NR predictions. This result agrees with the notion that the axial component associated with fully reversed torsion becomes more significant for larger twist angles.

On the basis of maximum normal strain, the multilevel tests (paths F and G) produced similar crack orientations as the corresponding constant amplitude tests. The maximum normal strain approach predicted zero-degree crack orientations for multilevel axial tests (path F). The predicted crack orientation for the multilevel torsion test in SBR is 26°, which is between the predicted crack orientations for the two twist angles that make up the signal.

The maximum normal strain accumulated damage results in Fig. 8 for test path H also show predicted cracking orientations between those of the individual cycles that make up the signal. These results range between 17° and 24° for SBR. Test signals involving higher numbers of axial to torsional cycles per sequence correspond to the lower crack angles while the higher crack angles have higher numbers of torsional cycles. The accumulated damage results for path I in Fig. 8 show a maximum damage value for the zero-degree plane for most of the tests. Only for the case of the highest number of torsion to axial cycles (7 torsion to 3 axial), a crack orientation other than zero degrees is predicted (5°).

Comparison of experimental and predicted crack orientations

Comparisons of the predicted and observed crack orientations are presented in Fig. 9 for NR and Fig. 10 for SBR.

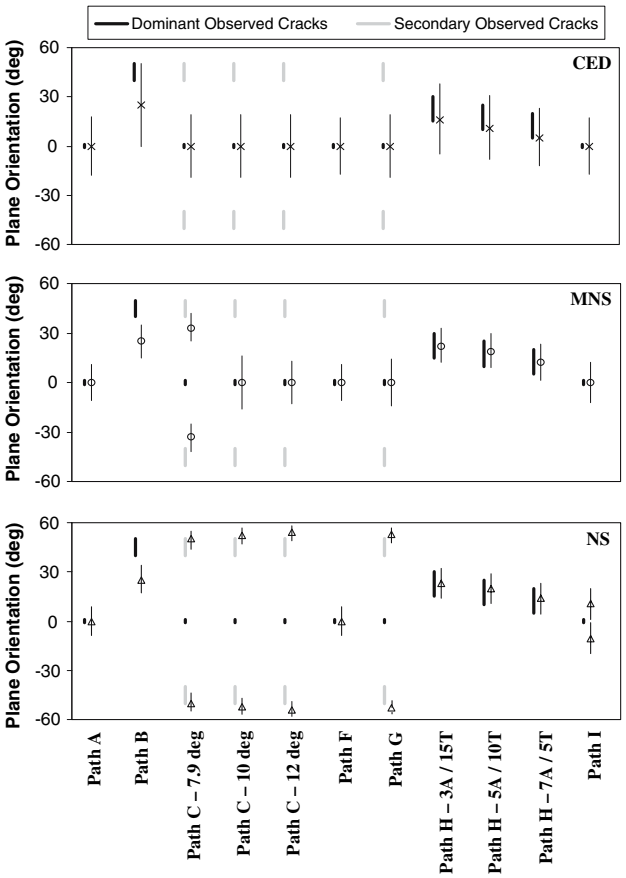

Fig. 9 Comparison of experimental and predicted crack orientations in NR for cracking energy density (CED), maximum normal strain (MNS), and normal strain (NS) range. The markers (×, ○, △) represent the predicted crack orientation of maximum damage while the lines represent the planes that are subjected to at least 95% of the maximum damage. The dominant cracks were the longest and most prevalent cracks

Both the dominant and secondary orientations of observed cracks are noted in these figures. Single points and lines are used for each test signal to indicate the predicted orientations of the maximum damage planes and the 95% damage ranges, respectively. All three approaches to predicting crack orientations were shown to be successful for some of the tests, while having difficulty capturing the effects of others.

For the cases of pure axial and multilevel axial tests (paths A and F), all of the approaches correctly predicted horizontal cracks for both materials. For the torsion tests with $R_\theta = 0$ (path B), all three approaches also correctly predicted angled cracks. Measured crack orientations were generally between 40° and 50° and the range of predicted crack orientations based on 95% of the maximum damage level for cracking energy density included the observed crack orientations while the other two approaches based on normal strain did not.

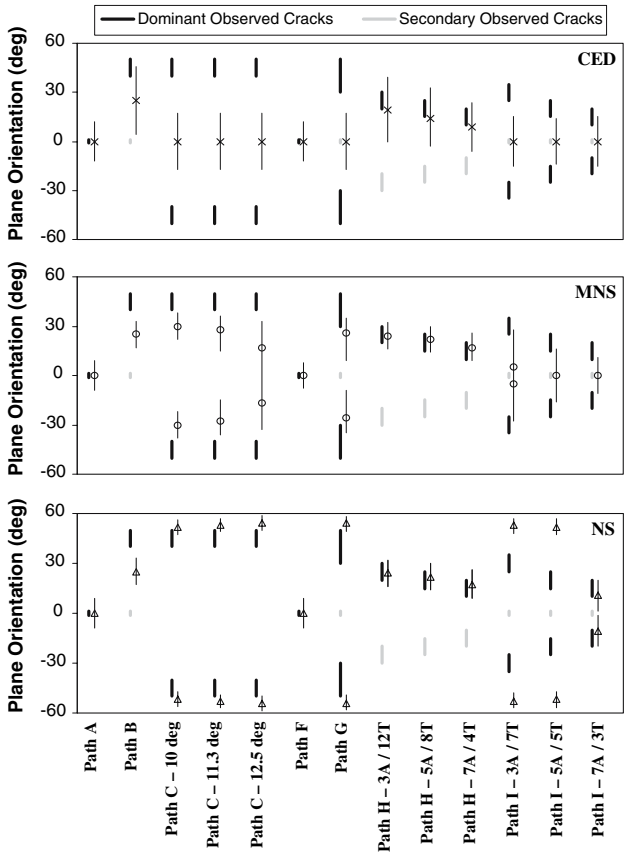

Fig. 10 Comparison of experimental and predicted crack orientations in SBR for cracking energy density (CED), maximum normal strain (MNS), and normal strain (NS) range. The markers (×, ○, △) represent the predicted crack orientation of maximum damage while the lines represent the planes that are subjected to at least 95% of the maximum damage. The dominant cracks were the longest and most prevalent cracks

The first significant difference observed between the approaches to predicting crack orientation occurred under conditions of fully reversed torsion (path C). Cracking energy density predicted horizontal cracks while the maximum normal strain predicted angled cracks for most of the tests. As noted in the previous section, the maximum normal strain predicts horizontal cracks in both materials for higher twist amplitudes. The normal strain range approach predicts angled cracks for all of the fully reversed torsion tests. The horizontal cracks observed for path C in NR agrees with the results for cracking energy density, but the angled cracks in SBR better agree with the normal strain range results. The maximum normal strain approach agrees with some of the cases for each material. Similar results were observed for the multilevel torsion tests (path G).

For the multiaxial tests combining axial and torsion with $R_\theta = 0$ (path H), all of the approaches correctly predicted angled cracks in the specimens for both materials. While the specific angles of crack orientation varied between the approaches, the predicted crack orientations generally fell within the range of angles observed experimentally. All of the approaches captured the observed sensitivity of the crack orientation to the relative number of axial and torsional cycles as observed during the experiments.

For test path I in NR, all three approaches correctly predicted the development of horizontal cracks. The dominant cracks in SBR for test path I were angled cracks that varied orientation with the number of axial and torsional cycles per sequence. Cracking energy density incorrectly predicted horizontal cracks for all of the variations of test path I in SBR. Similarly, maximum normal strain also predicted horizontal cracks for all of the variations in SBR except for the signal with the highest number of torsional cycles. The normal strain range predicted angled cracks that were higher than the observed crack orientations.

As previously discussed, multiple orientations experience similar levels of damage as indicated by the range of orientations for the 95% damage level. On the basis of the damage plots presented in Fig. 6 through Fig. 8 and the comparison of experimental and predicted crack orientations in Figs. 9 and 10, it is evident that the predicted range of orientations experiencing at least 95% of the damage is larger for cracking energy density than either of the normal strain approaches.

On the basis of the results presented in this section, all of the approaches have been shown to be capable of capturing several aspects of crack orientation well. However, none of the approaches were able to correctly predict the crack orientations for all of the tests in both materials.

Conclusions

(1) NR tended to produce a high density of smaller cracks while SBR generally produced a few small cracks that grew much larger before the failure of the specimen. This difference in crack development in the material was attributed to the difference in initial flaw size and density observed from microscopic images of the surface of the two materials.

(2) Axial tests (path A) produced only horizontal cracks in both materials, while torsion tests with $R_\theta = 0$ (path B) produced dominantly angled cracks between 40° and 50°. The observed crack orientations differed between the two materials for fully reversed torsion tests (path C). The NR specimens produced dominant horizontal cracks while the SBR specimens developed angled cracks in the positive and negative directions. This difference was attributed to the variation in flaw size and density between the materials.

(3) Multiaxial tests that combined axial and torsional cycles that acted on different planes (paths H and I) produced crack orientations that fell between the crack orientations of the individual cycles. The angle of crack orientation was related to the relative number of axial and torsional cycles per test sequence. More axial cycles generally produced crack orientations closer to zero while a higher number of torsional cycles produced higher angles of crack orientation.

(4) The plane-specific parameters of cracking energy density and normal strain were used to predict crack orientation ranges based on 95% of the maximum damage. Both cracking energy density and normal strain approaches were able to accurately predict the dominant crack orientations for some of the test signals in each material, but were inaccurate for others. Both approaches were able to capture the sensitivity of the multiaxial signals to the relative number of axial and torsional cycles per sequence in both materials well.

References

1. Sun C, Gent AN, Marteny P (2000) Tire Sci Technol 28:196
2. Roland CM, Sobieski JW (1989) Rubber Chem Technol 62:683
3. Klenke D, Beste A (1987) Kautsch Gummi Kunst 40:1067
4. Mars WV, Fatemi A (2005) Fatigue Fract Eng Mater Struct 28:523
5. Mars WV, Fatemi A (2006) J Mater Sci 41:7324
6. Mars WV, Fatemi A (2007) Rubber Chem Technol 80:169
7. Roland CM (1989) Rubber Chem Technol 62:863
8. Mars WV, Fatemi A (2004) Exp Mech 44:136
9. Miner MA (1945) J Appl Mech 6:159
10. Mars WV, Fatemi A (2005) Fatigue Fract Eng Mater Struct 28:515